HHS Public Access

Author manuscript

J Neurosci Res. Author manuscript; available in PMC 2017 November 01.

Published in final edited form as:

J Neurosci Res. 2017 May ; 95(5): 1225–1236. doi:10.1002/jnr.23954.

Mesenchymal stem cells attenuate MRI-identifiable injury, protect white matter and improve long-term functional outcomes after neonatal focal stroke in the rat

Cindy van Velthoven[1,*], **Mark Dzietko**[1,*], **Michael F. Wendland**[1], **Nikita Derugin**[1], **Joel Faustino**[1], **Cobi J. Heijnen**[2], **Donna M. Ferriero**[1,3], and **Zinaida S. Vexler**[1]

[1]Department of Neurology, University of California San Francisco, San Francisco, California, USA

[2]Laboratory of Neuroimmunology, Division of Internal Medicine, The University of Texas MD Anderson Cancer Center, Houston, Texas, USA

[3]Department of Pediatrics, University of California San Francisco, San Francisco, California, USA

Abstract

Cell therapy has emerged as a potential treatment for many neurodegenerative diseases including stroke and neonatal ischemic brain injury. Delayed intranasal administration of mesenchymal stem cells (MSC) after experimental hypoxia-ischemia and after a transient middle cerebral artery occlusion (tMCAO) in neonatal rats has shown improvement in long-term functional outcomes, but the effects of MSC on white matter injury (WMI) are insufficiently understood.

In this study we utilized longitudinal T2W and diffusion tensor MRI to characterize chronic injury after tMCAO induced in postnatal day 10 (P10) rats and examined the effects of delayed MSC administration on WMI, axonal coverage and long-term somatosensory function. We show unilateral injury- and region- dependent changes in diffusion fraction anisotropy 1 and 2 weeks after tMCAO that correspond to accumulation of degraded myelin basic protein, astrocytosis, and decreased axonal coverage. With the use of stringent T2W–based injury criteria at 72 hours after tMCAO to randomize neonatal rats to receive intranasal MSC or vehicle, we show that a single MSC administration attenuates WMI and enhances somatosensory function 28 days after stroke. A positive correlation was found between MSC-enhanced white matter integrity and functional performance in injured neonatal rats. Collectively these data indicate that the damage induced by tMCAO progresses over time and is halted by administration of MSC.

Graphical Abstract

Corresponding Author: Zinaida S. Vexler, Ph.D., University California San Francisco, Department of Neurology, 675 Nelson Rising Lane, San Francisco, CA 94158-0663, Tel (415) 502-2282, Fax (415) 502-5821, Zena.Vexler@ucsf.edu.

*contributed equally

Conflict of Interest: None

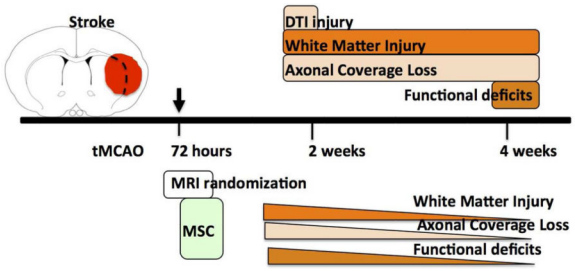

Keywords

perinatal stroke; brain repair; middle cerebral artery occlusion; axon; diffusion tensor imaging; fractional anisotropy

Introduction

Brain connectivity depends on correct myelination of axons (Nave and Werner 2014). At term getational age, the human brain is not yet fully myelinated, and perinatal stroke and hypoxic-ischemic encephalopathy (HIE) compromise myelination. Insufficient and delayed myelination contributes to cerebral palsy, long-term cognitive impairment and other neurological deficits (Back, Gan et al. 1998, McQuillen and Ferriero 2004). Rodent hypoxia-ischemia (H–I) studies clearly demonstrate that the stage of brain immaturity at the time of injury—preterm vs. term—plays a key role in the underlying WMI largely because of differing developmental oligodendrocyte arrest (Back, Riddle et al. 2007). Adverse effects of WMI on repair after neonatal H-I have been firmly established. However, the changed balance between negative and positive regulators of myelination such as disrupted oligoprogenitor differentiation, the contribution of individual pathways, malfunction of myelinating astrocytes, and disturbed cell-cell communications is far from understood (Fancy, Chan et al. 2011).

Therapeutic and repair potential for cell- based therapies, including mesenchymal stem cells (MSC), has been demonstrated in multiple neurodegenerative disease models in adult rodents, including stroke, brain trauma, and spinal cord injury. MSC improve functional outcomes after stroke (Chen, Li et al. 2003, Zhang, Li et al. 2004, Zacharek, Chen et al. 2007, Bliss, Andres et al. 2010, Daadi, Davis et al. 2010, Horie, Pereira et al. 2011) and traumatic brain injury (Mahmood, Lu et al. 2004) in the adult. In neonatal H-I, a surrogate for human HIE, MSC administration enhances brain repair in term models of neonatal H-I in postnatal day 7 (P7) mice (van Velthoven, Kavelaars et al. 2010, van Velthoven, Kavelaars et al. 2010, van Velthoven, Kavelaars et al. 2010, Donega, Nijboer et al. 2014, Donega, Nijboer et al. 2015). MSC also improve functional outcomes in focal arterial stroke induced by a transient middle cerebral artery occlusion (tMCAO) in P10 rats (van Velthoven, Sheldon et al. 2013).

One potential caveat in evaluating long-term repair after neonatal stroke is the variable extent of spontaneous recovery over time in rats with similar volume of abnormal diffusion-weighted imaging (DWI) signal during MCAO (Derugin, Wendland et al. 2000, Derugin,

Dingman et al. 2005, Dzietko, Faustino et al. 2011). In the context of the present study we sought out to determine the extent of the spatial changes of WMI after neonatal tMCAO and the relationship between MSC-mediated improvement of functional outcomes and WMI. To address the first question we utilized a combination of DWI during MCAO and longitudinal T2-weighted (T2W) MRI and diffusion tensor imaging (DTI) to non-invasively characterize progression of chronic injury after tMCAO in relation to WMI and axonal damage. We then applied stringent T2W inclusion and exclusion criteria for MSC/vehicle groups to evaluate the effects of MSC on long-term functional outcomes in relation to WMI, axonal injury and overall injury.

Materials and Methods

All animal experiments were approved by the Institutional Animal Care and Use Committee of the University of California, San Francisco, and every effort was made to minimize animal suffering and reduce the number of animals used. Sprague-Dawley dams with litter were purchased from Charles River Laboratories (Wilmington, MA, USA, RRID: RGD_737891). Mothers were housed in a temperature and light-controlled facility and given food and water.

Transient MCAO model in P10 rats

P10 rats of both sexes underwent a transient 1.5 hour right MCAO using surgical procedure as we originally described for P7 rats (Derugin, Dingman et al. 2005) and modified for P10 rats (Mu, Jiang et al. 2003, Dzietko, Faustino et al. 2011). Briefly, surgery was performed on spontaneously breathing pups anesthetized with 1.75% isoflurane in a mixture of 70% N_2O and 30% O_2. A small arteriotomy was made in the internal carotid artery and a coated 6-0 Dermalon filament was inserted and advanced 7.5 to 8.5 mm, depending on the animal's weight, and secured with a temporary sutured. The filament was removed 1.5 hours later to reestablish blood flow. A total of 35 rat pups from 8 litters were subjected to tMCAO. Most rat pups showed poor suckling during the first 2–3 days following surgery and were fed with 0.5ml of reconstituted commercial evaporated milk 3 times daily for 3 days.

MR Imaging

P10 rats underwent initial DWI screening during tMCAO, as we previously described (Derugin, Dingman et al. 2005, Dzietko, Faustino et al. 2011). For all MRI studies, rats were anesthetized with 1.75% isoflurane, placed on an acrylic bed and wrapped in a water heating pad to maintain core temperature and placed in a face mask with bite bar, secured with tape to minimize breathing motion during MRI and the head inserted into a 3.2 cm i.d. birdcage coil. Rats with evidence of characteristic pattern of DWI hyperintensity were used in further experiments.

T2W conventional spin echo multislice images (TR/TE = 3000/50ms) covering the entire brain with consecutive 1mm coronal sections with FOV = 2.56 cm, and data matrix of 128×128 points (0.2 mm in-plane pixel dimension) were obtained at 7T (Varian DirectDrive™ system, Varian, Inc.) Out of 11 rats from 3 litters planned for DTI-based characterization of evolution of ischemic injury, 9 rats met inclusion criteria; a full DTI set

was obtained only at a single time point in 3 rats, and motion artifacts precluded data analysis in 2 rats. Therefore, DTI was acquired in 4 rats at P18 and P25 with evidence of injury on DWI during MCAO and on T2W at P18. For DTI imaging TR/TE was 3000/50 msec, other settings were the same as for T2W MRI and the entire brain covered with 1mm thick contiguous coronal sections. Diffusion weighting with b-factors set to 730–760 s/mm^2, was applied along 6 non-coplanar axes: xy, yz, xz, x(-)y, (-)yz, and (-)xz axes. Each of the set of 7 images was acquired in 12.8 min for a total of 90 min acquisition time.

MR image analysis

FSL software, version 4.1.5 (downloaded from fsl.fmrib.ox.ac.uk, RRID:SCR_002823), was used to calculate DTI maps, including fractional anisotropy (FA), amplitude of mean diffusivity (trace), axial diffusivity (ADC along principal axis), and radial diffusivity along the 2 minor axes orthogonal to axial diffusivity, as well as associated vector maps for axial and radial diffusivities. Regions of interest (ROI) were chosen to evaluate signal intensities and apparent diffusion coefficients for ipsilateral and contralateral brain regions, as shown on Figure 1. Data quantification was performed in two anterior coronal sections in the injured caudate, less injured perifocal caudate and the corpus callosum (areas 1, 2, and 3 respectively) and in the corresponding contralateral areas (Figure 1D). No analysis was done at more posterior sections which are more sensitive to motion artifacts.

MSC treatment protocol

Rats with evidence of injury involving the ipsilateral caudate and cortex after MCAO and no injury in atypical regions like the brain stem or without cortical involvement on DWI during MCAO and on T2W MRI at 72 hours after tMCAO were randomized to receive Rat Sprague-Dawley MSC (GIBCO) or vehicle (PBS). MSC were negative for myeloid and hematopoietic cell lineage–specific antigens and positive for CD29, CD44, CD90, and CD106. Thirty minutes before MSC or vehicle administration, 2 doses of 5-μl hyaluronidase (Sigma-Aldrich) in PBS were applied to each nostril and spontaneously inhaled (van Velthoven, Kavelaars et al. 2010). Subsequently, a total of 1×10^6 MSC in 20μl PBS or vehicle were applied to each nostril to awake rats as 2 doses of 5 μl. A total of 24 rat pups from 5 litters were included into the study. Six pups died within 3 days after tMCAO (survival was 87%). 21 rats were subjected T2W on day 3 post-tMCAO/sham, Data are derived from: Sham-VEH n=5, Sham-MSC n=6, MCAO-VEH n=13, MCAO-MSC n=11. 13 rat pups subjected to tMCAO met inclusion criteria and were included in the study.

Histology, gliosis quantification and white matter lesion

P25 or P38 rats were sacrificed by transcardiac perfusion with ice-cold 0.1 M PBS followed by perfusion-fixation with ice-cold 4% paraformaldehyde in 0.1 M PBS. For the 2-week outcome study brains were post-fixed in the same solution overnight, cryoprotected in 30% sucrose in 0.1 M PBS and submerged for 3 days. Rat brains were flash frozen and coronal 12 μm-thick sections cut on a cryostat. Sections were stained with mouse-anti-GFAP (BD Biosciences, RRID:AB_396365), anti-BrdU antibody Abcam, RRID:AB AB6326) and isolectin-B4 (IB4, LifeTechnologies, RRID:AB_2314662). Z-stacks of 17 images acquired at 1 μm intervals (25x objective, Plan-Apo lens, NA 0.75), using a Zeiss Imager fluorescence microscope equipped with Volocity Software (Improvision, RRID:SCR_002668), were

deconvolved and analysis was performed in three ROIs in the ischemic (Area 1, Fig. 2F) and peri-infarct area (Area 2, Fig. 2F) of the caudate and in the ipsilateral uninjured cortex (Area 3, Fig. 2F). Matching contralateral ROIs served as internal controls. We used automated protocols for signal intensity threshold of GFAP (>2 SD background in each channel; Volocity Software), as previously described (Faustino, Wang et al. 2011). Adjacent sections were incubated with rabbit-anti-degraded MBP (dMBP) (Millipore, RRID:AB_2140351) or mouse-anti-Neurofilament H (NFH) non-phosphorylated (Millipore, RRID: AB_2043449) followed by donkey-anti-mouse-AlexaFluor488 or donkey- anti-rabbit-AlexaFluor488 (LifeTechologies). Images were analyzed using FIJI(RRID:SCR_002285). For the 1-month outcomes brains were paraffin-embedded, cut coronal (10 μm), deparaffinized and immunostained for MBP (mouse-MBP; Sternberger Monoclonals, RRID: AB_2140494), dMBP and NFH using similar immunolabeling protocols. Positive staining was calculated as percentage of positive area per total hemisphere. Reagent details are provided in Table 1.

Somatosensory testing protocol

The cylinder rearing test was used to assess forelimb asymmetry at 28 days post-MCAO as previously described (van Velthoven, Sheldon et al. 2013). The animal was placed in a transparent cylinder and videotaped. Each session consisted of 3 minutes in the cylinder or a minimum of 20 upright wall contacts. The weight-bearing forepaw(s) to contact the wall during a full rear was recorded as left (impaired), right (nonimpaired), or both. Paw preference was calculated as (nonimpaired-impaired)/(nonimpaired forepaw+impaired forepaw+both)×100.

Statistical Analysis

Analyses were performed using Prism 6 (Graphpad Software, RRID:SCR_002798). All data are shown as mean ± SEM. Grouped data were analyzed using 2-way ANOVA to determine statistical differences between results, and if deemed significant Bonferroni post hoc analysis was used to test between specific groups. NFH and dMBP staining were analyzed using student's t-test. Differences were considered significant at $p<0.05$. The relation between injury severity and impairment in the cylinder rearing test was analyzed by Pearson's correlation.

Results

Transient MCAO in P10 rats leads to unilateral chronic T2W and DTI changes

Considering that a highly reproducible injury pattern delineated by DWI during tMCAO is followed by a variable extent of T2W and histological injury later (72 hours – 2 weeks) (Derugin, Dingman et al. 2005, Dzietko, Faustino et al. 2011), in this study we identified injured pups on DWI during MCAO (Figure 1C) and performed T2W at 1 week after MCAO to select rats with persistent severe injury for DTI measurements. Typical T2W injury patterns included hypointense regions in ipsilateral caudate and cortex, thinning of ipsilateral cortex and asymmetric enlargement of lateral ventricle space ipsilateral to the ischemic injury, consistent with loss of tissue in the injured region (Figure 1E). Compared to the size of normal appearing caudate/putamen in three consecutive slices centered at the anterior commissure, the size of normal appearing ipsilateral caudate/putamen, i.e.,

excluding hypointense regions on T2W images, was reduced to 27±7% of the contralateral side.

In rats with evidence of T2W abnormalities at P18, full DTI protocol was performed at P18 and P25, because, in naïve brain, white matter maturation culminates during the third week of postnatal rodent life. WMI during this period might also critically affect functional performance, angiogenesis and neurogenesis in post-ischemic brain. Moreover, DTI images/maps showed clearly defined white matter structures with apparent shift of internal capsule. Vectors maps and maps of axial diffusivity and FA were generated. DTI provided sufficient contrast to delineate rostral normal appearing caudate/putamen (Figure 1E). ROIs chosen for data analysis of DTI parameters (shown on Figure 1B) were applied at P18 (Table 2 and Figure 1E) and P25 (Table 2 and Figure 1F).

In the contralateral hemisphere, FA values were significantly different between the caudate and corpus callosum (CC) at each of two time points studied (Table 2). Significantly higher FA values in the CC compared to the gray matter during the same developmental time in rodents are consistent with previously reports (Mori and Zhang 2006), but not in the same regions between P18 and P25 (Table 2). Significantly increased FA values were seen in the injured caudate (Area 1, Figure 1D and Table 2) but not in the less injured perifocal caudate region (Area 2, Figure 1) or in the CC (Area 3, Figure 1) when compared to the uninjured contralateral side. The magnitude of change was also affected by imaging coordinates, as seen for anterior and posterior section (Figure 1D and Table 2). Measurements at 1 and 2 weeks after tMCAO showed similar results in the same ipsilateral ROIs (Figure 1D).

Chronic injury involves gliosis and white matter degradation

To determine the extent of morphological injury in rats with evidence of DTI abnormalities, we determined reactive astrogliosis, the presence of degraded MBP and axonal coverage. A strong glial response was observed 2 weeks after tMCAO. GAFP+ cells co-localized with IB4+ macrophages in the scar. Continued cell proliferation was observed within the car. $GFAP^+$ coverage was most prominent in the post-ischemic caudate and in the cortical ischemic core (Figure 2C,G). Accumulation of GFAP+ cells was significantly higher in the injured and peri-infarct region of the caudate compared to the contralateral side and to the ipsilateral uninjured cortex at P25 (Figure 2D,E); the density of $GFAP^+$ areas was lower compared to the core region.

Accumulation of dMBP was observed in 5.46±1.05% of the ipsilateral hemisphere compared to 2.27±0.74% in the contralateral hemisphere ($p<0.05$, Figure 2). NFH^+ area in the ipsilateral hemisphere was 3.38±0.62% compared to 9.35±1.52 in the contralateral hemisphere ($p<0.05$).

Delayed MSC treatment protects WM and axonal coverage and attenuates functional outcomes

We then asked if MSC protect the neonatal brain from WMI. To evaluate the repair potential of MSC rather than protection, we postponed MSC administration until 72 hours after tMCAO, a time point when acute caspase-3-dependent and independent neuronal death reach their peak and begin to decline in directly injured regions (Manabat, Han et al. 2003).

Although DWI-identifiable injury volume is consistent during MCAO (Derugin, Dingman et al. 2005, Dzietko, Faustino et al. 2011), over time injury volume ranges in individual rat pups from largely unchanged to markedly reduced. To avoid bias while examining long-term outcomes of MSC effects, we used T2W during sub-chronic injury to randomize rats to receive MSC/vehicle. As evident from T2W MRI, rats included into this study had similar T2W injury size at the time of treatment, including significant damage to the cortex and striatum (Figure 3A). Quantitative analysis showed that injury volume before MSC/vehicle administration was not significantly different between the two treatment groups regardless whether injury volume was determined across all 7 coronal slices (Figure 3B) or only at the level of the caudate (Figure 3C).

NFH coverage, an indicator of axonal presence, was significantly increased by MSC-treatment at 28 days post tMCAO when compared to vehicle-treated rats (Figure 4A,B). Treatment with MSC provided significant protection from MBP degradation compared to vehicle-treated rats (Figure 4C,D). Preservation of MBP was associated with significantly higher preserved ipsilateral MBP and NFH expression (Figure 4E).

Previous somatosensory results, measured by the cylinder rearing test, have shown that tMCAO causes lateralization, as vehicle-treated rats have a higher preference for the right unimpaired forepaw (van Velthoven, Sheldon et al. 2013). Following treatment with MSC, such lateralizing behavior significantly decreased when compared to vehicle-treated rats (Figure 5). An unbiased MRI-based randomization of rat pups established that the severity of the ischemic brain injury, as measured by total ipsilateral volume by Nissl staining and MBP degradation, positively correlated with improved lateralizing motor deficits in MSC-treated rats (Figure 5A and C respectively), linking MBP preservation to improved functional performance. No significant relationship between ipsilateral NFH expression and motor function was detected (Figure 5B).

Discussion

This study illustrates, for the first time, region-specific changes in average water diffusivity and FA in relation to chronic ischemic injury and WMI in injured neonatal rats after stroke. An unbiased MRI-based randomization of rat pups with subchronic ischemic injury for MSC treatment showed that MSC enhance WM integrity and improved functional performance at 1 month after the insult.

In humans, DTI, including diffusion tensor tractography (DTT), has allowed mapping and quantification of WM tracts of injured premature newborns (Partridge, Mukherjee et al. 2005) and shows a strong correlation between corticospinal tract DTI changes with motor outcome in children with perinatal stroke (Roze, Harris et al. 2012).

In mouse and rat brains, FA maps derived during the embryonic, early and late neonatal periods demonstrate a relatively high anisotropy (0.3–0.5) in the premyelinated cortex and WM and reciprocal changes in the gray and WM during myelination. Further increases in FA values in the WM are likely due to myelination of axons and/or increase in axonal density in the first 2 weeks after birth (Mori and Zhang 2006). The only available DTI data

related to experimental neonatal cerebral ischemia-related injuries come from hypoxia-ischemia (H–I) studies. Ex vivo DTI demonstrate selective injury to WM tracts, axonal loss and progressive deterioration of remote regions (ipsilateral fimbria) within 5 weeks after H-I in P7 mice (Stone, Zhang et al. 2008) and show correlation between changes in FA in the CC and MBP expression and performance on Morris water maze test 3–11 weeks after H-I in P9 mice (Cengiz, Uluc et al. 2011). While DTI of a motionless injured brain provides incredible resolution and identifies changes in WM tracts, ex vivo DTI may overestimate the magnitude of changes and does not provide information on injury progression. When applied to living immature P3 rats subjected to H-I, DTI at 24 and 72 hours shows changes in radial organization, disappearance of radial organization with the deep layers maturing earlier than the external layers, and associated changes in cortical architecture by histology (Sizonenko, Camm et al. 2007). DTI applied at 24 hours (Lodygensky, West et al. 2011) or 3 hours – 4 weeks (Tuor, Morgunov et al. 2014) after H-I in P7 rats shows region-dependent and time-dependent abnormalities. Changes are more subtle early and more extensive at 2–4 weeks after H-I and are observed in a directly damaged region, cerebral cortex, and in a region with secondary axonal degeneration, the cerebral peduncle. DTI changes are associated with reduced myelination, reactive astrocytes, microgliosis and neuronal death (Tuor, Morgunov et al. 2014). At one day after H-I, only reduction in both axial and radial directions was shown to represent severe damage associated with loss of structural integrity and necrosis (Wang, Wu et al. 2008). At 10 weeks, a significantly lower FA but higher axial, radial and mean diffusivities are observed in the ipsilateral CC, proximal external capsule and anterior commissure (Chan, Khong et al. 2009), suggesting that increased FA, axial and mean diffusivity characterize WM reorganization in chronic neonatal H-I insults.

We also observe significantly increased FA values in the injured caudate compared to FA values in adjacent perifocal regions or in contralateral caudate regions. Multiple factors could contribute to the increase in FA values in the caudate, including delayed WM development during brain maturation, abnormal axons, and a glial scar. The relative contribution of these factors to directionality of water movement is not well understood. Extensive glial scarring and dysmyelination (or delay in myelination) and axonal injury could also be consistent with low FA signal due to reduced water content in the developing scar. While in the WM motion of water molecules is aligned due to the structural environment, the directionality of axons is difficult to interpret due to different fiber orientations averaged over a large voxel volume. Moreover, axial diffusivity is greater and radial diffusivities smaller for ipsilateral versus contralateral caudate, with no difference in mean diffusivity, and the principal vector direction is mostly superior-inferior, consistent with a putative dense fibrillar structure with long axis aligned along the principle direction.

Interestingly, we do not observe significant FA changes in the ipsilateral CC. It is unknown whether changes in the CC are affected by the timing after injury, by rat age at time of injury, or by the model, H-I vs. tMCAO. Comparisons of our data in injured P10 rats with existent data in the H-I model in P7 rats is further affected by ongoing WM maturation during a narrow age range (reviewed in (Semple, Blomgren et al. 2013)). One limitation in FA data interpretation is that there are restrictions in correlating MRI observations to the underlying neuroanatomy because of thicker MR slices and heterogeneity of tissue. Although tissue pathology underlying ischemic and degenerative responses has a complex

relationship with DTI parameters, our DTI results are in agreement with morphological and histological results, i.e., the reduced myelination, accumulation of degraded MBP and reduced axonal coverage observed. FA changes, marked astrogliosis and accumulation of damaged MBP at 2 weeks are associated with significant somatosensory and motor abnormalities at the same time point after tMCAO in P10 rats (van Velthoven, Sheldon et al. 2013).

Our immunohistochemical results indicate that, while ipsilateral axonal injury does not change from two to four weeks after tMCAO, there is an increase in WM degradation during this period. Delayed MSC treatment attenuates WM degradation. WM and oligodendrocyte precursor cells are highly vulnerable to ischemic brain injury (Pantoni, Garcia et al. 1996, Back, Han et al. 2002, Arai, Lok et al. 2011). WMI causes oligodendrocyte cell arrest and axonal myelination failure. The latter impairs axonal conduction and causes motor, sensory and cognitive deficits (Duncan, Brower et al. 2009). Following ischemia-induced dysmyelination, oligodendrogenesis is stimulated in an attempt to remyelinate the damaged region. Oligodendrocyte precursor cells start proliferating and migrate to the lesion. This response peaks at 5 to 7 days after the insult and subsides between 14 and 28 days after the insult (Zaidi, Bessert et al. 2004, Iwai, Stetler et al. 2010). Once at the site of injury, the oligodendrocyte precursor cells need to differentiate and start myelinating axons. However, ischemic injury has been shown to block maturation of oligodendrocytes leading to myelination failure (Billiards, Haynes et al. 2008, Syed, Baer et al. 2008).

Oligodendrogenesis is tightly regulated by extrinsic signals coming from the microenvironment (reviewed by (Fancy, Chan et al. 2011)). The disturbance in the microenvironment caused by ischemic injury is likely a major cause for disturbed maturation of oligodendrocytes (Franklin and Ffrench-Constant 2008). Treatment with MSC after ischemic brain injury has been shown to alter the ischemic microenvironment in the brain and improve various endogenous repair processes (van Velthoven, Kavelaars et al. 2010, Liu, Ye et al. 2014). In response to MSC treatment following ischemia, there is an increase in oligodendrocyte precursor cells, mature oligodendrocytes and increased myelin formation (van Velthoven, Kavelaars et al. 2010, van Velthoven, Sheldon et al. 2013). Furthermore, MSC secrete factors that promote oligodendroglial fate determination in neural progenitor cells in vitro (Rivera, Couillard-Despres et al. 2006). MSC treatment in this model of neonatal stroke could also alter other aspects of microenvironment in the ischemic hemisphere, thereby preventing myelination arrest.

MSC can be successfully delivered to the immature brain non-invasively by the nasal route (van Velthoven, Kavelaars et al. 2010) and migrate into the brain and accumulate predominantly in the infarcted area. Delayed intranasal administration of MSC after neonatal stroke significantly enhanced somatosensory function 14, 21 and 28 days after tMCAO, reduced tissue loss and improved motor function 28 days after tMCAO (van Velthoven, Sheldon et al. 2013). MSC are shown to reduce infarct size by >45%, stimulate formation of new neurons and oligodendrocytes, partially restore cortico-spinal motor tract activity, and improve sensorimotor outcome (van Velthoven, Kavelaars et al. 2010, van Velthoven, Kavelaars et al. 2010). While there is a lot of excitement about enhanced MSC-induced brain repair, the underlying mechanisms are not fully understood. There is

considerable evidence that MSC exert brain repair after adult and neonatal brain injury in part by changing the brain microenvironment. Intravenous MSC reduce apoptosis, promote endogenous cell proliferation (Chen, Li et al. 2003), significantly reduce the expression of inhibitory factors in astrocytes, including a broad array of glycoproteins, (Shen, Li et al. 2008) but also increase production of growth factors, including VEGF and BDNF (Zacharek, Chen et al. 2007). Angiopoietin1/Tie2 and VEGF/Flk1 induced by MSC amplify angiogenesis, a process necessary for remodeling and neuroblast migration (Zacharek, Chen et al. 2007). Importantly, in the neonatal H-I model, while MSC protect injured brain and enhance functional outcomes, the survival of MSC sharply declines to only 1% 18 days after delivery (van Velthoven, Kavelaars et al. 2011). However, MSC markedly affect gene expression of growth factors and inflammatory molecules (van Velthoven, Kavelaars et al. 2011).

Recent studies in other neurodegenerative diseases, like multiple sclerosis, have shown that MSC act by reshaping the brain microenvironment (Giunti, Parodi et al. 2013, Laroni, Novi et al. 2013), in part by microglial (Giunti, Parodi et al. 2013) and oligodendrocyte behavior (Jaramillo-Merchan, Jones et al. 2013). MSC administration in a cuprizone model of de- and remyelination without the influence of the peripheral immune system did not increase remyelination, suggesting that the peripheral immune system is required for MSC (especially T cells) to exert their effects (Salinas Tejedor, Berner et al. 2015). Our functional outcome data at one month in rats with similar injury severity at the time of MSC administration show a positive correlation with WM preservation by MSC but lack of significant correlation with axonal coverage. These data suggest that attenuation of WMI by MSC is an important factor in long-term repair.

While the underlying mechanisms of MSC-mediated brain repair continue to be insufficiently understood, our data show that combined assessment of T2W-detectible injury and FA directionality maps allow differentiating chronic effects of neonatal stroke and recovery quantitatively and non-invasively and are useful in drug translational studies. Further, our data expand our previously published observations by linking MSC-enhanced white matter integrity to enhance somatosensory function 28 days after neonatal arterial focal stroke.

Acknowledgments

Acknowledgements of Funding Resources

The work was supported by NS35902 (DMF and ZSV), RO1 NS55915 (ZSV), RO1 NS44025 (ZSV), RO1 NS76726 (ZSV)

Author's roles: All listed authors met criteria for authorship, as recommended by the ICMJE

Other Acknowledgments: The authors acknowledge Ann Sheldon for coordinating MRI and animal studies.

References

Arai K, Lok J, Guo S, Hayakawa K, Xing C, Lo EH. Cellular mechanisms of neurovascular damage and repair after stroke. J Child Neurol. 2011; 26(9):1193–1198. [PubMed: 21628695]

Back SA, Gan X, Li Y, Rosenberg PA, Volpe JJ. Maturation-dependent vulnerability of oligodendrocytes to oxidative stress-induced death caused by glutathione depletion. J Neurosci. 1998; 18(16):6241–6253. [PubMed: 9698317]

Back SA, Han BH, Luo NL, Chricton CA, Xanthoudakis S, Tam J, Arvin KL, Holtzman DM. Selective vulnerability of late oligodendrocyte progenitors to hypoxia-ischemia. J Neurosci. 2002; 22(2):455–463. [PubMed: 11784790]

Back SA, Riddle A, McClure MM. Maturation-dependent vulnerability of perinatal white matter in premature birth. Stroke. 2007; 38(2 Suppl):724–730. [PubMed: 17261726]

Billiards SS, Haynes RL, Folkerth RD, Borenstein NS, Trachtenberg FL, Rowitch DH, Ligon KL, Volpe JJ, Kinney HC. Myelin abnormalities without oligodendrocyte loss in periventricular leukomalacia. Brain Pathol. 2008; 18(2):153–163. [PubMed: 18177464]

Bliss TM, Andres RH, Steinberg GK. Optimizing the success of cell transplantation therapy for stroke. Neurobiol Dis. 2010; 37(2):275–283. [PubMed: 19822211]

Cengiz P, Uluc K, Kendigelen P, Akture E, Hutchinson E, Song C, Zhang L, Lee J, Budoff GE, Meyerand E, Sun D, Ferrazzano P. Chronic neurological deficits in mice after perinatal hypoxia and ischemia correlate with hemispheric tissue loss and white matter injury detected by MRI. Dev Neurosci. 2011; 33(3–4):270–279. [PubMed: 21701150]

Chan KC, Khong PL, Lau HF, Cheung PT, Wu EX. Late measures of microstructural alterations in severe neonatal hypoxic-ischemic encephalopathy by MR diffusion tensor imaging. Int J Dev Neurosci. 2009; 27(6):607–615. [PubMed: 19505567]

Chen J, Li Y, Katakowski M, Chen X, Wang L, Lu D, Lu M, Gautam SC, Chopp M. Intravenous bone marrow stromal cell therapy reduces apoptosis and promotes endogenous cell proliferation after stroke in female rat. J Neurosci Res. 2003; 73(6):778–786. [PubMed: 12949903]

Daadi MM, Davis AS, Arac A, Li Z, Maag AL, Bhatnagar R, Jiang K, Sun G, Wu JC, Steinberg GK. Human neural stem cell grafts modify microglial response and enhance axonal sprouting in neonatal hypoxic-ischemic brain injury. Stroke. 2010; 41(3):516–523. [PubMed: 20075340]

Derugin N, Dingman A, Wendland M, Fox C, Vexler ZS. Magnetic Resonance Imaging as a Surrogate Measure for Histological Sub-Chronic Endpoint in a Neonatal Rat Stroke Model. Brain Res. 2005; 1066:49–56. [PubMed: 16336947]

Derugin N, Wendland M, Muramatsu K, Roberts T, Gregory G, Ferriero D, Vexler Z. Evolution of brain injury after transient middle cerebral artery occlusion in neonatal rat. Stroke. 2000; 31:1752–1761. [PubMed: 10884483]

Donega V, Nijboer CH, Braccioli L, Slaper-Cortenbach I, Kavelaars A, van Bel F, Heijnen CJ. Intranasal administration of human MSC for ischemic brain injury in the mouse: in vitro and in vivo neuroregenerative functions. PLoS One. 2014; 9(11):e112339. [PubMed: 25396420]

Donega V, Nijboer CH, van Velthoven CT, Youssef SA, Bruin Ade, van Bel F, Kavelaars A, Heijnen CJ. Assessment of long-term safety and efficacy of intranasal mesenchymal stem cell treatment for neonatal brain injury in the mouse. Pediatr Res. 2015; 78(5):520–526. [PubMed: 26270577]

Duncan ID, Brower A, Kondo Y, Curlee JF Jr, Schultz RD. Extensive remyelination of the CNS leads to functional recovery. Proc Natl Acad Sci U S A. 2009; 106(16):6832–6836. [PubMed: 19342494]

Dzietko M, Faustino J, Derugin N, Wendland MF, Ferriero DM, Vexler ZS. MRI as a Translational Tool for the Study of Neonatal Stroke. J Child Neurol. 2011; 26(9):1145–1153. [PubMed: 21670390]

Fancy SP, Chan JR, Baranzini SE, Franklin RJ, Rowitch DH. Myelin regeneration: a recapitulation of development? Annu Rev Neurosci. 2011; 34:21–43. [PubMed: 21692657]

Faustino J, Wang X, Jonhson C, Klibanov A, Derugin N, Wendland M, Vexler ZS. Microglial cells contribute to endogenous brain defenses after acute neonatal focal stroke. J Neurosci. 2011; 31(36):12992–13001. [PubMed: 21900578]

Franklin RJ, Ffrench-Constant C. Remyelination in the CNS: from biology to therapy. Nat Rev Neurosci. 2008; 9(11):839–855. [PubMed: 18931697]

Giunti D, Parodi B, Cordano C, Uccelli A, Kerlero de Rosbo N. Can we switch microglia's phenotype to foster neuroprotection? Focus on multiple sclerosis. Immunology. 2013

Horie N, Pereira MP, Niizuma K, Sun G, Keren-Gill H, Encarnacion A, Shamloo M, Hamilton SA, Jiang K, Huhn S, Palmer TD, Bliss TM, Steinberg GK. Transplanted stem cell-secreted vascular endothelial growth factor effects poststroke recovery, inflammation, and vascular repair. Stem Cells. 2011; 29(2):274–285. [PubMed: 21732485]

Iwai M, Stetler RA, Xing J, Hu X, Gao Y, Zhang W, Chen J, Cao G. Enhanced oligodendrogenesis and recovery of neurological function by erythropoietin after neonatal hypoxic/ischemic brain injury. Stroke. 2010; 41(5):1032–1037. [PubMed: 20360553]

Jaramillo-Merchan J, Jones J, Ivorra JL, Pastor D, Viso-Leon MC, Armengol JA, Molto MD, Geijo-Barrientos E, Martinez S. Mesenchymal stromal-cell transplants induce oligodendrocyte progenitor migration and remyelination in a chronic demyelination model. Cell Death Dis. 2013; 4:e779. [PubMed: 23990019]

Laroni A, Novi G, Kerlero de Rosbo N, Uccelli A. Towards clinical application of mesenchymal stem cells for treatment of neurological diseases of the central nervous system. J Neuroimmune Pharmacol. 2013; 8(5):1062–1076. [PubMed: 23579931]

Liu X, Ye R, Yan T, Yu SP, Wei L, Xu G, Fan X, Jiang Y, Stetler RA, Liu G, Chen J. Cell based therapies for ischemic stroke: from basic science to bedside. Prog Neurobiol. 2014; 115:92–115. [PubMed: 24333397]

Lodygensky GA, West T, Moravec MD, Back SA, Dikranian K, Holtzman DM, Neil JJ. Diffusion characteristics associated with neuronal injury and glial activation following hypoxia-ischemia in the immature brain. Magn Reson Med. 2011; 66(3):839–845. [PubMed: 21394776]

Mahmood A, Lu D, Chopp M. Intravenous administration of marrow stromal cells (MSCs) increases the expression of growth factors in rat brain after traumatic brain injury. J Neurotrauma. 2004; 21(1):33–39. [PubMed: 14987463]

Manabat C, Han BH, Wendland M, Derugin N, Fox CK, Choi J, Holtzman DM, Ferriero DM, Vexler ZS. Reperfusion differentially induces caspase-3 activation in ischemic core and penumbra after stroke in immature brain. Stroke. 2003; 34(1):207–213. [PubMed: 12511776]

McQuillen PS, Ferriero DM. Selective vulnerability in the developing central nervous system. Pediatr Neurol. 2004; 30(4):227–235. [PubMed: 15087099]

Mori S, Zhang J. Principles of diffusion tensor imaging and its applications to basic neuroscience research. Neuron. 2006; 51(5):527–539. [PubMed: 16950152]

Mu D, Jiang X, Sheldon RA, Fox CK, Hamrick SE, Vexler ZS, Ferriero DM. Regulation of hypoxia-inducible factor 1alpha and induction of vascular endothelial growth factor in a rat neonatal stroke model. Neurobiol Dis. 2003; 14(3):524–534. [PubMed: 14678768]

Nave KA, Werner HB. Myelination of the nervous system: mechanisms and functions. Annu Rev Cell Dev Biol. 2014; 30:503–533. [PubMed: 25288117]

Pantoni L, Garcia JH, Gutierrez JA. Cerebral white matter is highly vulnerable to ischemia. Stroke. 1996; 27(9):1641–1646. discussion 1647. [PubMed: 8784142]

Partridge SC, Mukherjee P, Berman JI, Henry RG, Miller SP, Lu Y, Glenn OA, Ferriero DM, Barkovich AJ, Vigneron DB. Tractography-based quantitation of diffusion tensor imaging parameters in white matter tracts of preterm newborns. J Magn Reson Imaging. 2005; 22(4):467–474. [PubMed: 16161075]

Rivera FJ, Couillard-Despres S, Pedre X, Ploetz S, Caioni M, Lois C, Bogdahn U, Aigner L. Mesenchymal stem cells instruct oligodendrogenic fate decision on adult neural stem cells. Stem Cells. 2006; 24(10):2209–2219. [PubMed: 16763198]

Roze E, Harris PA, Ball G, Elorza LZ, Braga RM, Allsop JM, Merchant N, Porter E, Arichi T, Edwards AD, Rutherford MA, Cowan FM, Counsell SJ. Tractography of the corticospinal tracts in infants with focal perinatal injury: comparison with normal controls and to motor development. Neuroradiology. 2012; 54(5):507–516. [PubMed: 22006424]

Salinas Tejedor L, Berner G, Jacobsen K, Gudi V, Jungwirth N, Hansmann F, Gingele S, Prajeeth CK, Baumgartner W, Hoffmann A, Skripuletz T, Stangel M. Mesenchymal stem cells do not exert direct beneficial effects on CNS remyelination in the absence of the peripheral immune system. Brain Behav Immun. 2015; 50:155–165. [PubMed: 26140734]

Semple BD, Blomgren K, Gimlin K, Ferriero DM, Noble-Haeusslein LJ. Brain development in rodents and humans: Identifying benchmarks of maturation and vulnerability to injury across species. Prog Neurobiol. 2013; 106–107:1–16.

Shen LH, Li Y, Gao Q, Savant-Bhonsale S, Chopp M. Down-regulation of neurocan expression in reactive astrocytes promotes axonal regeneration and facilitates the neurorestorative effects of bone marrow stromal cells in the ischemic rat brain. Glia. 2008; 56(16):1747–1754. [PubMed: 18618668]

Sizonenko SV, Camm EJ, Garbow JR, Maier SE, Inder TE, Williams CE, Neil JJ, Huppi PS. Developmental changes and injury induced disruption of the radial organization of the cortex in the immature rat brain revealed by in vivo diffusion tensor MRI. Cereb Cortex. 2007; 17(11): 2609–2617. [PubMed: 17259644]

Stone BS, Zhang J, Mack DW, Mori S, Martin LJ, Northington FJ. Delayed neural network degeneration after neonatal hypoxia-ischemia. Ann Neurol. 2008; 64(5):535–546. [PubMed: 19067347]

Syed YA, Baer AS, Lubec G, Hoeger H, Widhalm G, Kotter MR. Inhibition of oligodendrocyte precursor cell differentiation by myelin-associated proteins. Neurosurg Focus. 2008; 24(3–4):E5.

Tuor UI, Morgunov M, Sule M, Qiao M, Clark D, Rushforth D, Foniok T, Kirton A. Cellular correlates of longitudinal diffusion tensor imaging of axonal degeneration following hypoxic-ischemic cerebral infarction in neonatal rats. Neuroimage Clin. 2014; 6:32–42. [PubMed: 25379414]

van Velthoven CT, Kavelaars A, van Bel F, Heijnen CJ. Mesenchymal stem cell treatment after neonatal hypoxic-ischemic brain injury improves behavioral outcome and induces neuronal and oligodendrocyte regeneration. Brain Behav Immun. 2010; 24(3):387–393. [PubMed: 19883750]

van Velthoven CT, Kavelaars A, van Bel F, Heijnen CJ. Nasal administration of stem cells: a promising novel route to treat neonatal ischemic brain damage. Pediatr Res. 2010; 68(5):419–422. [PubMed: 20639794]

van Velthoven CT, Kavelaars A, van Bel F, Heijnen CJ. Repeated mesenchymal stem cell treatment after neonatal hypoxia-ischemia has distinct effects on formation and maturation of new neurons and oligodendrocytes leading to restoration of damage, corticospinal motor tract activity, and sensorimotor function. J Neurosci. 2010; 30(28):9603–9611. [PubMed: 20631189]

van Velthoven CT, Kavelaars A, van Bel F, Heijnen CJ. Mesenchymal stem cell transplantation changes the gene expression profile of the neonatal ischemic brain. Brain Behav Immun. 2011; 25(7):1342–1348. [PubMed: 21473911]

van Velthoven CT, Sheldon RA, Kavelaars A, Derugin N, Vexler ZS, Willemen HL, Maas M, Heijnen CJ, Ferriero DM. Mesenchymal stem cell transplantation attenuates brain injury after neonatal stroke. Stroke. 2013; 44(5):1426–1432. [PubMed: 23539530]

Wang S, Wu EX, Tam CN, Lau HF, Cheung PT, Khong PL. Characterization of white matter injury in a hypoxic-ischemic neonatal rat model by diffusion tensor MRI. Stroke. 2008; 39(8):2348–2353. [PubMed: 18535275]

Zacharek A, Chen J, Cui X, Li A, Li Y, Roberts C, Feng Y, Gao Q, Chopp M. Angiopoietin1/Tie2 and VEGF/Flk1 induced by MSC treatment amplifies angiogenesis and vascular stabilization after stroke. J Cereb Blood Flow Metab. 2007; 27(10):1684–1691. [PubMed: 17356562]

Zaidi AU, Bessert DA, Ong JE, Xu H, Barks JD, Silverstein FS, Skoff RP. New oligodendrocytes are generated after neonatal hypoxic-ischemic brain injury in rodents. Glia. 2004; 46(4):380–390. [PubMed: 15095368]

Zhang J, Li Y, Chen J, Yang M, Katakowski M, Lu M, Chopp M. Expression of insulin-like growth factor 1 and receptor in ischemic rats treated with human marrow stromal cells. Brain Res. 2004; 1030(1):19–27. [PubMed: 15567334]

Significance statement

This study demonstrates, for the first time, region-specific changes on diffusion-tensor imaging (DTI) in relation to chronic ischemic injury and white matter abnormalities after neonatal focal arterial stroke. T2W-MRI used during sub-chronic injury to randomize rats with similar injury to receive mesenchymal stem cells (MSC)/vehicle has allowed us to expand the understanding of the MSC-improved one-month outcome and link enhanced somatosensory function to enhanced white matter integrity.

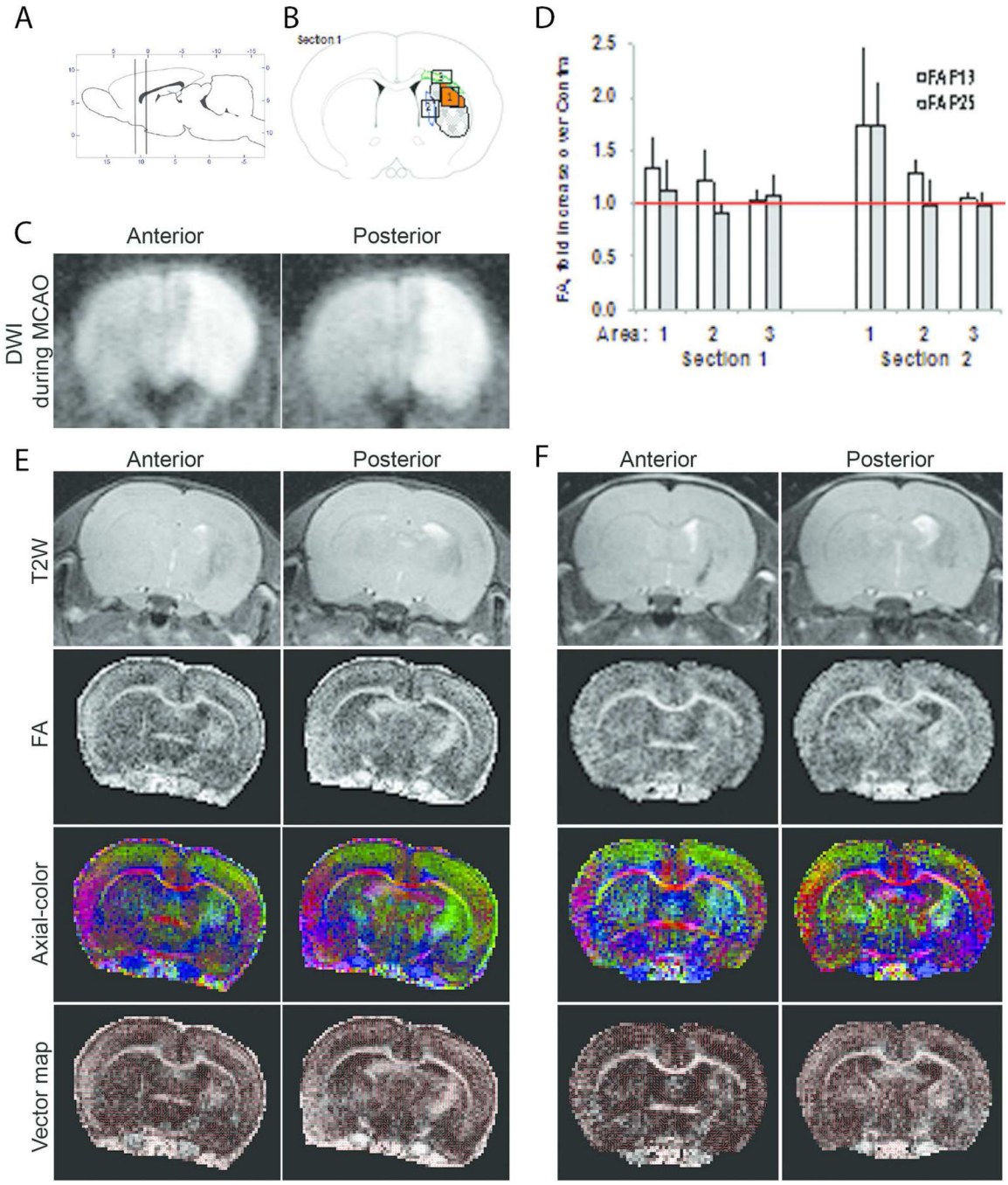

Figure 1. MRI-based demarcation of injury evolution after tMCAO in P10 rats

A. Diagram indicating the position of the transverse slices depicted in C, D and E and the areas used for measurement of FA values. B. A diagram of the ROIs used for data analysis. ROIs were chosen based on reduced signal intensity on T2W images in injured hemisphere in the injured caudate (Area 1), injured perifocal caudate (Area 2), and in white matter of the CC to external capsule (Area 3). C. Representative DWI images from one animal obtained during occlusion on anterior and posterior levels. D. FA values measured in Areas 1–3 compared to matching areas in the contralateral hemisphere at the level of the anterior

commissure and a more posterior plane. Data shown as mean±SEM and were analyzed using a paired Students t-test. n=4. *p<0.05 contralateral vs. ipsilateral. Detailed data are shown in Table 2. E-F. Representative images at p18 (E) and at p25 (F) at the level of the anterior commissure and at the posterior level. Shown are: DWI, T2W images, FA maps; color-coded representation of the axial vector map (principal eigenvector map) superimposed on the FA map, with green coloration representing superior-inferior axis, red coloration representing left-right axis, and blue coloration representing rostral-caudal axis; and vector map in which the direction of the principle eigenvector is represented by equal line lengths in each pixel, which appear shorter when through-plane component is important, overlaid on the FA maps.

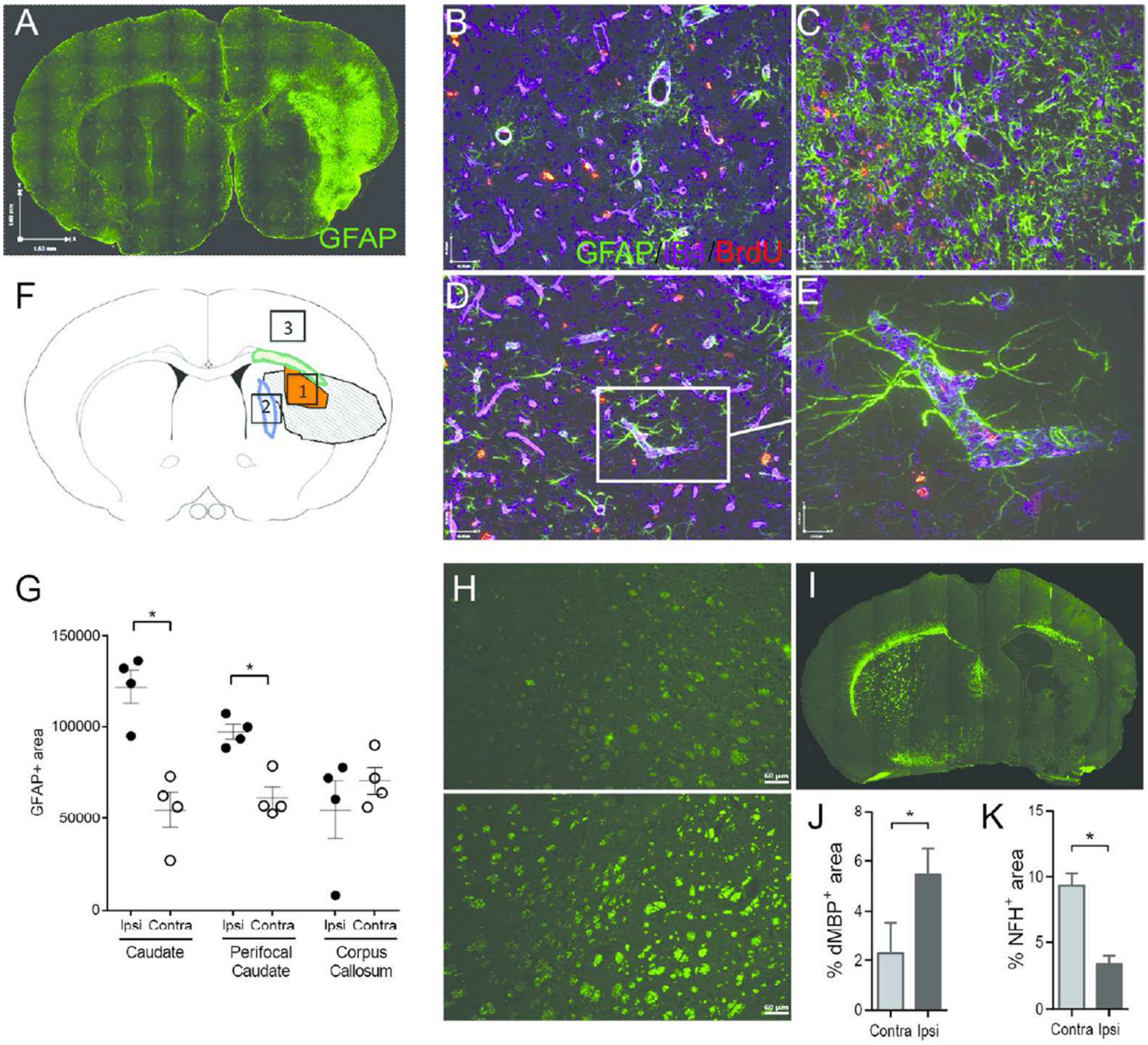

Figure 2. Glial scar and accumulation of damaged MBP at 2 weeks after tMCAO

A- G. The spatial distribution of reactive GFAP$^+$ astrocytes (A, stitched image). GFAP$^+$ astrocytes are predominantly seen adjacent to the vessels in contralateral cortex (B) and caudate (D). Profound GFAP accumulation is observed in the ischemic caudate (C, Area 1 on the diagram, F). Scale bars for B-D represent 40 μM. A high power image of the peri-infarct region shows the proximity of GFAP$^+$ cells to the vessels and BrdU$^+$ cells (E). Scale bar represents 10 μM.. F. A diagram of a coronal section with outlined areas 1–3 used for data analysis in the ipsilateral hemisphere. Matching anatomical regions in the contralateral hemisphere served as internal control. G. Quantification of astrogliosis represented by GFAP$^+$ signal intensity in the ipsilateral cortex compared to the contralateral region. H. Examples of dMBP+-areas in contralateral (top) and ipsilateral (bottom) caudate. Scale bar represents 60μM. I. Stitched image of NFH+ coronal brain section. J. Quantification of

dMBP accumulation in the entire hemisphere. K. Quantification of NFH coverage in the entire hemisphere. For J. and K. Data represent mean±SEM and were analyzed using a paired Students t-test. n=4. *p<0.05 contralateral vs. ipsilateral.

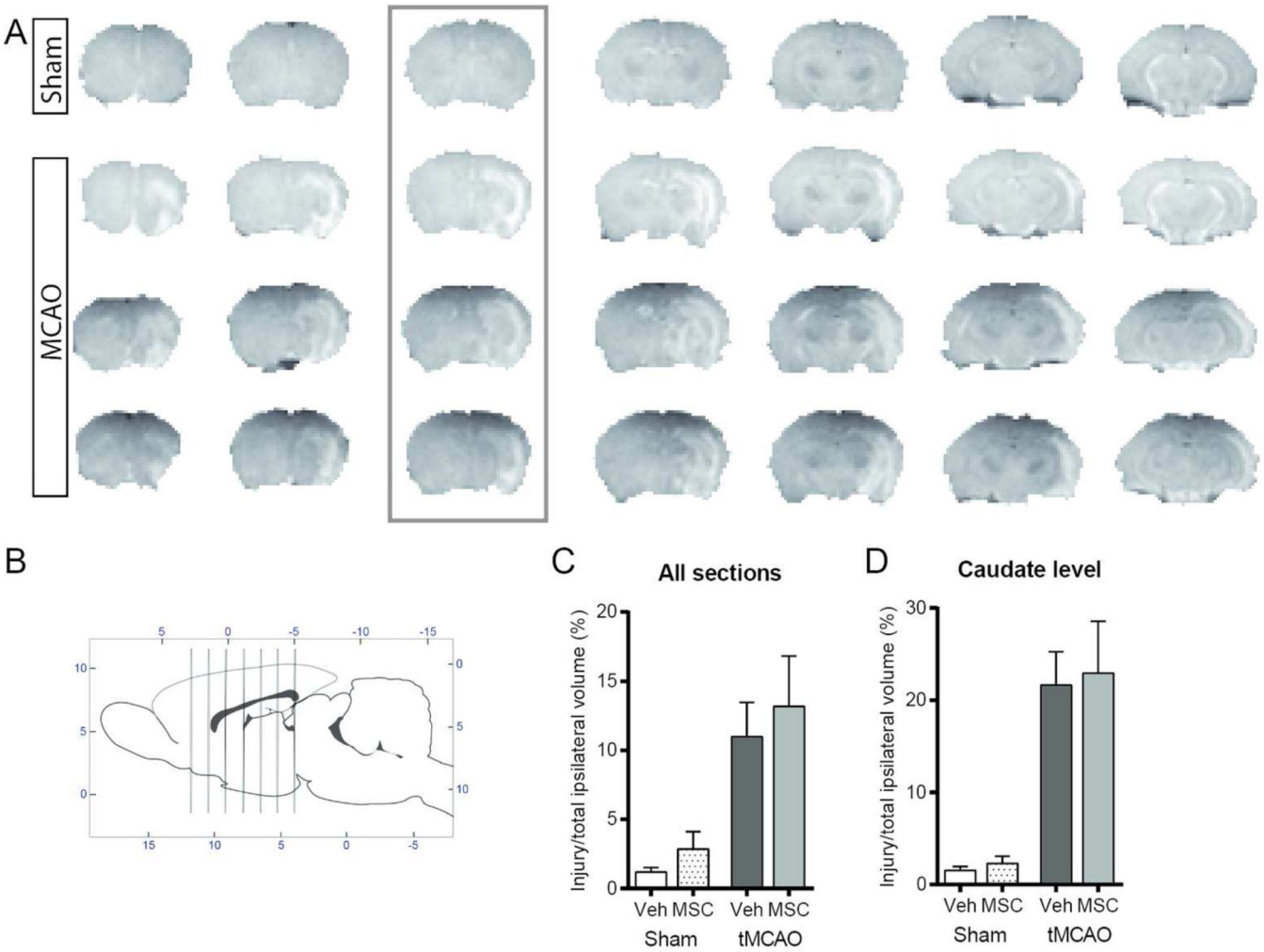

Figure 3. T2W –based injury patterns in rats selected for treatment groups 72 hours after tMCAO

A. Representative examples of T2W MRI for sham (top row) and tMCAO (lower 3 rows). Shown are 7 consecutive anterior-to-posterior images. B. Schematic indicating the position of the transverse slices depicted in A. C. T2W injury volume measured in all seven coronal sections. D. T2W injury volume measured at the caudate level (coronal section indicated by the box). Volume of injury was similar in rats that received MSC and vehicle. Data were analyzed using 2-way ANOVA, $F(1,30)=0.1906$ n = x; $P=0.6657$. Dots correspond to the data from individual rats (n=6–7/group).

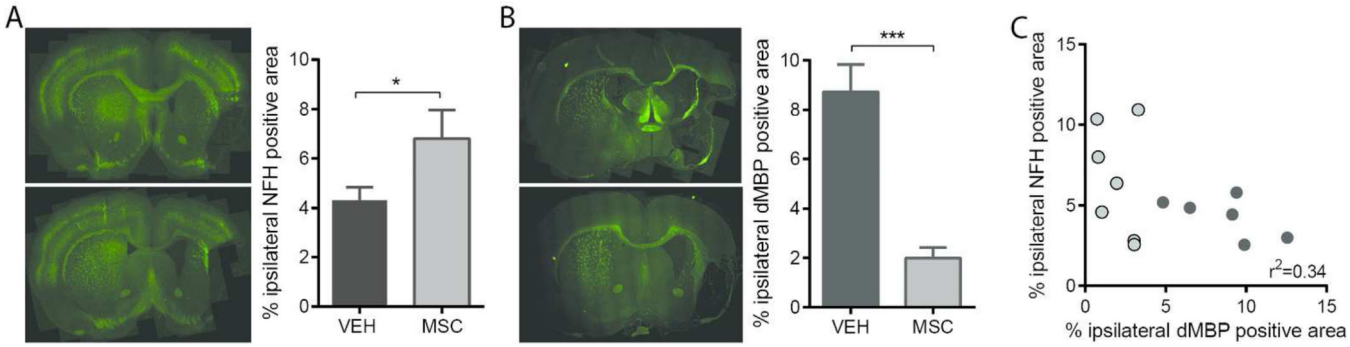

Figure 4. MSC administration attenuates white matter loss 28 days after tMCAO

A. Representative images of brain sections immunolabeled for NFH and quantification of ipsilateral NFH coverage.B. Representative images of brain sections immunolabeled for iMBP staining andquantification of dMBP coverage in the injured hemisphere. C. Relation between NFH-positive area and dMBP-positive area in ipsilateral. VEH n=6, MSC n=7. Data was analyzed using a one-tailed t test *p<0.05 MSC vs VEH, ***p<0.001 MSC vs VEH. Pearson's r^2=0.34, p<0.05.

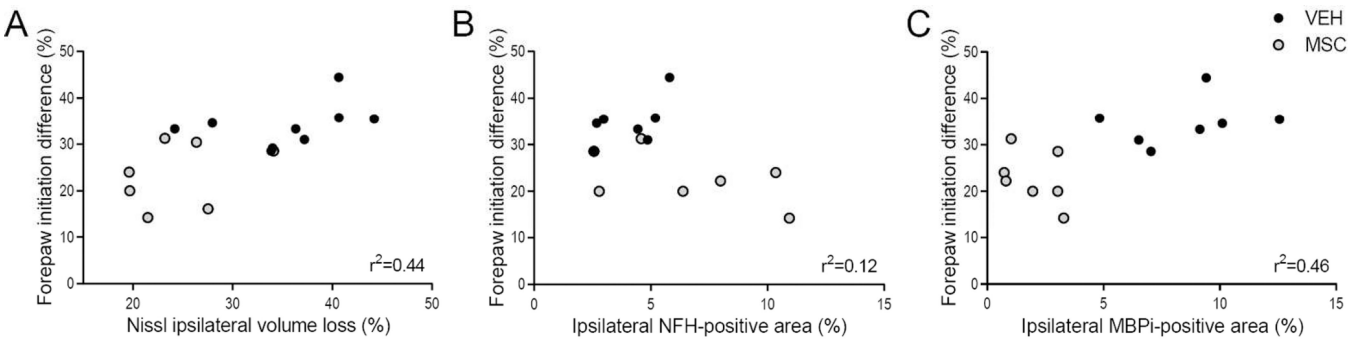

Figure 5. Relationships between injury severity and lateralizing motor deficits in MSC and vehicle-treated rats

A. Relationship between forepaw initiation difference at p28 and ipsilateral volume loss. VEH n=9, MSC n=7. Pearson's r^2=0.44, p<0.05. B. Relationship between forepaw initiation difference at p28 and ipsilateral NFH-positive area. VEH n=7, MSC n=7. Pearson's r^2=0.12, p=NS. C. Relationship between forepaw initiation difference and ipsilateral dMBP-positive area. VEH n=7, MSC n=7. Pearson's r^2=0.46, p<0.01.

Table 1

Antigen	Description of Immunogen	Source, Catalog No., RRID	Host Specis, Clone, Concentration used
GFAP	Cow spinal cord homogenate	BD Bioscience, 556327, AB_396365	Mouse, 4A11, 1:200
IB4	a 114,000-dalton glycoprotein that is part of a family of five tetrameric type I isolectins (IA_4, IA_3B, IA_2B_2, IAB_3, and IB_4) isolated from the seeds of the tropical African legume *Griffonia simplicifolia*.	Molecular Probes, I21411, AB_2314662	1:100
BrdU	Anti-BrdU antibody	ab6326; BU1/75 (ICR1)	1:200
MBP	Recombinant fragment corresponding to amino acids 70–89 of Human Myelin Basic Protein	Millipore, NE1018, AB_2140494	Mouse, SMI-94, 1:500
dMBP	Synthetic peptide corresponding to amino acids 69–86 of the guinea pig protein	Millipore, AB5864, AB_2140351	Rabbit, 1:200
NFH	homogenized hypothalami from Fischer 344 rat brain	Millipore, NE1023, AB_2043449	Mouse, SMI-32,1:500

Table 2

DTI characteristics 1 and 2 weeks after tMCAO

P18							
Anterior commissure		**axial ADC**	**radial-1 ADC**	**radial-2 ADC**	**Trace**	**FA**	
[1]	**Ipsi**	0.00114	0.00080	0.00058	0.00084	**0.33**	**P=0.018**
[2]	**Ipsi**	0.00112	0.00080	0.00062	0.00085	**0.29**	**ns**
[3]	**Ipsi**	0.00126	0.00078	0.00044	0.00083	**0.46**	**ns**
[4]	**Contra**	0.00098	0.00077	0.00059	0.00078	**0.25**	
[5]	**Contra**	0.00100	0.00080	0.00061	0.00080	**0.25**	
[6]	**Contra**	0.00123	0.00081	0.00043	0.00083	**0.45**	
1mm Posterior							
[1]	**Ipsi**	0.00112	0.00069	0.00049	0.00076	**0.40**	**P=0.024**
[2]	**Ipsi**	0.00111	0.00076	0.00053	0.00080	**0.36**	**ns**
[3]	**Ipsi**	0.00142	0.00066	0.00038	0.00082	**0.57**	**ns**
[4]	**Contra**	0.00097	0.00077	0.00058	0.00077	**0.25**	
[5]	**Contra**	0.00107	0.00082	0.00061	0.00083	**0.28**	
[6]	**Contra**	0.00140	0.00072	0.00040	0.00083	**0.54**	
P25							
Anterior commissure		**axial ADC**	**radial-1 ADC**	**radial-2 ADC**	**Trace**	**FA**	
[1]	**Ipsi**	0.00110	0.00078	0.00054	0.00081	**0.35**	**ns**
[2]	**Ipsi**	0.00111	0.00082	0.00060	0.00084	**0.30**	**ns**
[3]	**Ipsi**	0.00136	0.00073	0.00034	0.00081	**0.56**	**ns**
[5]	**Contra**	0.00103	0.00075	0.00052	0.00077	**0.32**	
[7]	**Contra**	0.00105	0.00078	0.00051	0.00078	**0.33**	
[8]	**Contra**	0.00129	0.00081	0.00035	0.00081	**0.52**	
1mm Posterior							
[1]	**Ipsi**	0.00128	0.00073	0.00041	0.00081	**0.50**	**P=0.02**
[2]	**Ipsi**	0.00108	0.00076	0.00054	0.00080	**0.34**	**ns**
[3]	**Ipsi**	0.00137	0.00075	0.00037	0.00083	**0.55**	**ns**

P18

	Anterior commissure	axial ADC	radial-1 ADC	radial-2 ADC	Trace	FA
[4]	**Contra**	0.00095	0.00073	0.00051	0.00073	**0.30**
[5]	**Contra**	0.00107	0.00080	0.00049	0.00079	**0.36**
[6]	**Contra**	0.00131	0.00071	0.00032	0.00078	**0.56**

Regions [1–3] correspond to ipsilateral regions shown in Figure 1C. [1] – ischemic core in the caudate; [2] – perifocal injury region; [3] – CC. [4–6] – respective contralateral regions.